Optimization of Finite-sized Modular Coils for Advanced Stellarators

Yangbo Li[1], Haifeng Liu[1,4*], Yuhong Xu[1], Akihiro Shimizu[2,3], Shigeyoshi Kinoshita[2], Shoichi Okamura[2], Mitsutaka Isobe[2,3], Guozhen Xiong[1], Yang Luo [1], Jun Cheng[2], Hai Liu[1], Xianqu Wang[1], Jie Huang[1], Xin Zhang[1], Dapeng Yin[5], Yi Wan[5], and Changjian Tang[1,4]

[1] *Institute of Fusion Science, School of Physical Science and Technology, Southwest Jiaotong University, Chengdu 610031, China*
[2] *National Institute for Fusion Science, National Institutes of Natural Sciences, Toki 509-5292, Japan*
[3] *The Graduate University for Advanced Studies, SOKENDAI, Toki 509-5292, Japan*
[4] *College of Physics, Sichuan University, Chengdu 610065, China*
[5] *Hefei Keye Electro Physical Equipment Manufacturing Co., Ltd, Hefei 230000, China*

Abstract

To date all coil-design codes, e.g. NESCOIL, COILOPT, FOCUS codes, etc., almost primarily attribute to optimization of filament coils for stellarators. However, evolving to a practical/finite-sized coil from a filament coil, the finite-size effect of coils significantly constrains fabrication tolerances of a coil system. This paper presents a novel approach that emphasizes the optimization of practical modular coils to reduce sensitivity to fabrication tolerances and to achieve the expected magnetic configurations precisely. A new evaluation parameter, surface twist, is defined in this paper and applied to the optimization sequence in addition to the practical coil line torsion and curvature. The approach has been applied to the framework of the filament coil scheme in the Chinese First Quasi-axisymmetric Stellarator (CFQS). This practical coil system without surface twists has been completely accomplished. Compared to the original finite-sized coil design, the new result is a more considerable simplification of coil shapes, such that in a certain direction view each finite-sized coil becomes planar-like one. Moreover, this method can also be implemented for the estimation of stochastic deviations of practical coils during fabrication and assembly of the coil system.

Key words: coil optimization, quasi-axisymmetric stellarator, finite-size effect of coils

1. Introduction

Stellarators[1] could achieve disruption-free, steady-state plasmas without requirement of the external current drive[2]. However, the stellarator concept also confronts significant challenges related to the complex coil system. The non-planar coils of a stellarator are dramatically difficult to design and fabricate due to the requirement of precise three-dimensional shaping[3]. The capability of non-planar coils to generate an appropriate magnetic configuration is constrained by the prerequisite that the adjacent coils can't be overlapped. In addition, the minimum coil-to-coil interval in stellarators is generally narrow, which limits access between the coils for installations of diagnostics and heating systems and for blanket maintenance as well[4]. Therefore, any advances in stellarator coil optimization can potentially bring remarkable impact on the practicability of magnetic confined fusion devices.

The modular coil system of stellarators (typically non-planar coils) has been employed for the achievement of various configurations[5]. The Wendelstein 7-X (W7-X), a quasi-isodynamic stellarator, comprises 50 non-planar and 20 planar modular coils which could robustly produce the quasi-isodynamic configuration [6,7]. The Helically Symmetric Experiment (HSX) is a quasi-helically symmetric (QHS) stellarator with 48 modular twisted coils. It is stably operating in America[8,9]. The Chinese First Quasi-axisymmetric Stellarator[10] (CFQS) under construction is developed by Southwest Jiaotong University(SWJTU) in China and National Institute for Fusion Science(NIFS) in Japan as an internationally collaborative project. The 16 modular coils have been designed to produce a quasi-axisymmetric magnetic field [11,12]. This paper concentrates on the optimization of the CFQS modular coil system.

Pioneering work on the field of coil design was performed by Merkel with the development of the NESCOIL code[13]. It is assumed that the external magnetic field is induced by a surface current distribution on a closed toroidal surface enclosing the plasma. The location of all coils is constrained by this toroidal surface which is called the 'current carrying surface' or the 'winding surface'. This method was successfully applied to the design of the coils of W7-X. However, due to the defective nature of inverting the Biot-Savart integrals, the NESCOIL results for the discrete coils for plasmas with complex shapes might not be viable. Although a singular value decomposition method[14] and a Tikhonov regularization approach[15] have been applied to provide improvements on NESCOIL， it only indirectly control the geometry

of the resultant coils set and allow limited opportunities to optimize the engineering constraints.

In order to explicitly incorporate and estimate engineering constraints the extended NESCOIL code [16] and ONSET code [17] have been developed by Drevlak. Strickler and Breslau *et al* developed the code COILOPT [18] and COILOPT + + [19]. Filament coils are optimized in these codes, which are embedded on a toroidal winding surface. The geometry of the coils is varied by nonlinear optimization algorithms to minimize a penalty-function that describes a balance between the physics requirement, i.e., the minimization of the total normal magnetic field on the plasma boundary and the engineering constraints which mainly include radius of coil curvature and distance between adjacent coils. Modular coil systems for the compact stellarators NCSX [20,21] and CHS-qa [22,23] were designed using this approach.

It is noted that a winding surface brings about strong limitations as well. A winding surface with an unfavorable shape directly gives rise to the failure of designing practical coils set. In other word, a favorable winding surface should first be obtained which is an access to finalize an acceptable coil set. However, the estimation of a winding surface with or without a favorable shape is dependent on the final coil geometries. The optimization sequences targeting both the winding surface and the coils are required. Recently, Caoxiang *et al* presented a new method to design stellarator coils without the winding surface and developed FOCUS code [24,25]. Each discrete coil is represented as an arbitrary, closed, one-dimensional curve in three-dimensional space. This method is capable to avoid the unnecessary constraints resulted from the dependence of a winding surface.

These codes mentioned above are merely appropriate for designing and optimizing the filament coils of stellarators. Nevertheless, the filament coils are not practical coils since each coil should be finite-sized to carry a current, inducing designed plasma configurations. From a filament coil to a finite-sized one, each coil cross section twists toroidally along the central line of a coil. Thus, how to finalize the twisted angle for each cross section is a critical issue on the generation of practical coils, since these twisted angles significantly constrain complexities of a coil shape and impact the precision of magnetic configurations if the size of coil cross sections is big. Few studies touch the process of the design of finite-sized coils. Therefore, a further approach to optimize a finite-sized coil system is urgently needed.

In this paper, we present a new method on optimizing the finite-sized coils for the CFQS. The configuration characteristics of the CFQS and the filament coil design and optimization are briefly shown in section 2. In section 3, the new strategy to optimize finite-sized coils is explained in detail. The optimization results are given in section 4. Conclusions are depicted in section 5.

2. Filament coil design of the CFQS

The main parameters of the CFQS are chosen as follows: the toroidal period number $N = 2$, major radius $R_0 = 1.0$ m and magnetic field strength $B_t = 1.0$ T and aspect ratio $A_p = 4.0$.[26] The toroidal period number $N = 2$ is selected, which guarantees to form the tokamak-like configuration[27-29]. The effect of components and economy is an important reason to choose a low aspect ratio for the CFQS design. The VMEC code is implemented to calculate the MHD equilibrium with a target fixed boundary and the magnetic field strength can be resolved with Fourier spectra $B_{m,n}$ in Boozer coordinates [30]. Additionally, the large toroidicity can reduce non-axisymmetric magnetic field components. The quasi-axisymmetry means that only the first row of coefficients $B_{m,0}$ plays a dominant role in the magnetic configuration. In Fig.1, the equilibrium of vacuum magnetic surfaces calculated by VMEC code[31].

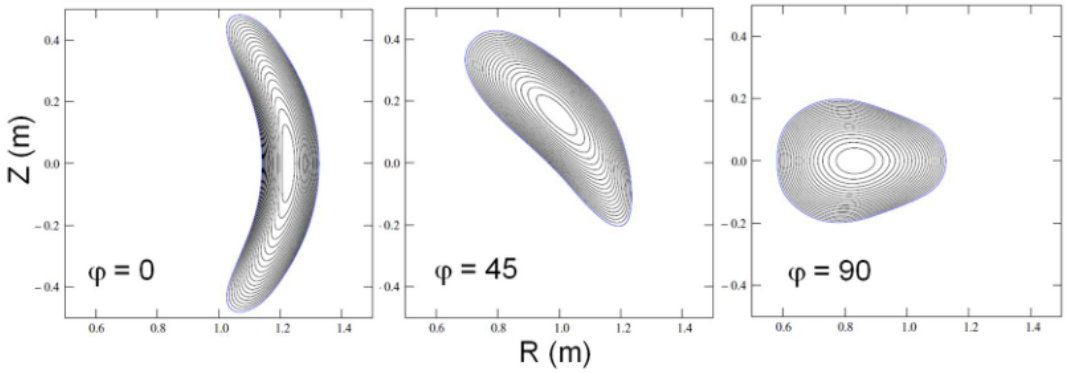

Fig. 1 CFQS vacuum magnetic surfaces calculated by VMEC code.

Vacuum equilibrium properties of a toroidal configuration are merely dependent on the shape of the outmost closed flux surface (plasma boundary). In order to achieve the target magnetic configuration, a modular coil system is necessary to be designed to reproduce the plasma boundary. Due to the Neumann boundary condition, the accuracy of the magnetic configuration induced by the coil system depends on the normal component of the magnetic field on the plasma boundary, which is expressed as $\mathbf{B} \cdot \mathbf{n}$

where **B** is the vacuum magnetic field generated from the coil system on the plasma boundary and **n** is the normal unit vector of this surface. Via the minimization of $\mathbf{B} \cdot \mathbf{n}$ on the plasma boundary, the modular coil geometry is optimized. Meanwhile, the engineering constraints are taken into account which are the minimum interval between adjacent coils and maximum coil curvature. They are under consideration to avoid the coil-coil overlap and reduce complexity of coil shapes. This design process is accomplished by the NESCOIL code. In the design of the coil system for the CFQS, the coil numbers, major radius and aspect ratio have been scanned to achieve an optimum modular coil system. Finally, the 16-coils system is preferable, which shows that the minimum interval between adjacent filament coils is the widest; the minimum radius of curvature is the largest and the magnetic flux surface generated is the closest to the target surface. Due to the toroidal period number N = 2 and stellarator symmetry, the whole torus consists of four symmetric sections. Fig. 2 (a) shows the modular coil system of the CFQS, including MC1-MC4 coils. Each section possesses four different shaped modular coils as shown in a magnetic surface coordinate in Fig. 2 (b). One can see that the most complex shape for the coils is MC4 coil nearby the cross-section at $\varphi = 90°$ (see Fig. 1). The interval between the centerline of any two coils exceeds 182.4 mm everywhere and the minimum radius of curvature is 173.7mm.

With respect to the engineering constrains of modular coils, besides coil-coil intervals and coil curvatures, another critical factor, surface twist, is of great importance, arising from the generation of finite-sized coils from filament coils. The concept, surface twist, may be defined for the first time in this paper, given in the Eq.(1). The following section illustrates how to generate and further simplify a set of practical modular coils in detail. In this optimization the 16 filament coils of the CFQS are produced by the NESCOIL code and fixed. The coil cross-section is rectangular and the area is 132.0×69.0 mm^2[32].

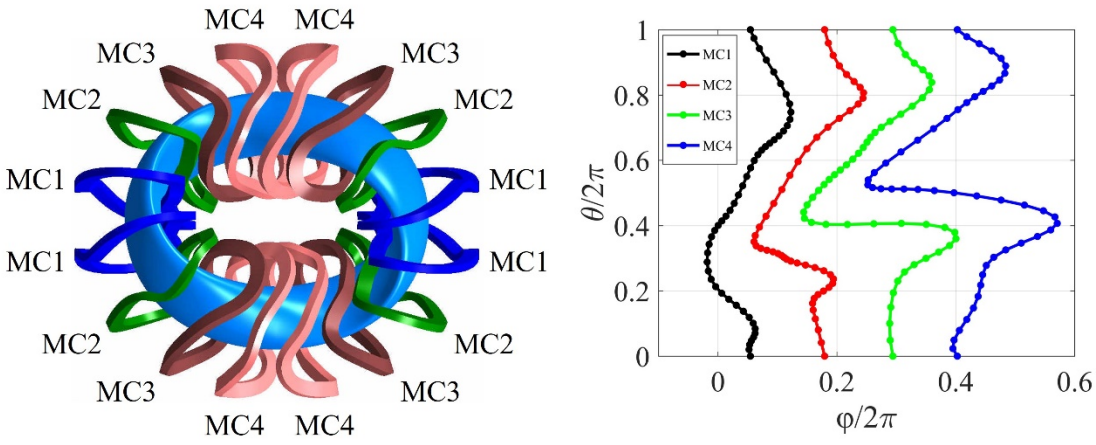

Fig. 2 The modular coil system of the CFQS (a). The center line of four different modular coils (MC1, MC2, MC3, MC4) of the CFQS in Boozer coordinate (b). The horizontal and vertical axes represent the toroidal and the poloidal angles, respectively.

3. Strategy to form practical coils

The engineering constrains of coil mainly include curvature radius of coils, line torsions of coils, the gap between adjacent coils and gap between coils and a vacuum vessel. In this paper, we have proposed a new evaluation parameter, surface twist, to optimize finite-sized coils. From a filament coil to a finite-sized one, a modular coil should be discretized poloidally and the number of coil cross-sections is given first. In the CFQS, 48 cross-sections for each modular coil are considered. For the original modular coils, without optimizations, each cross-section of the coil is merely guaranteed perpendicular to the current carrying surface. However, during the generation of practical modular coils, it is found that the original coils have significant surface twists which have a substantial influence on the fabrication tolerances and magnetic configurations. This torsion can also result in error fields, unfavourite curvature, etc., in case that the area of coil cross-section is large. In order to figure out this crucial issue, two types of torsions are defined: the line torsion, a conventional parameter, which has been used in the Frenet–Serret frame[33] and the surface twist which is a novel parameter and defined in this paper for the first time to our knowledge.

Regarding finite-sized coils, here exist three types of twists between adjacent cross-sections as displayed in Fig. 3. Fig. 3 (a) shows a part of finite-sized coils with the surface twist. The surface twist denotes the toroidal twist scale of a cross-section

relative to the adjacent cross-section. Figs. 3 (b) and (c) give other two kinds of twists without surface twists, i.e. flatwise and edgewise bending, respectively. These three kinds of twists are independent of each other and the latter two are not avoidable for non-planar coils. Favorably, the former one, the surface twist, can be eliminated via appropriate optimizations.

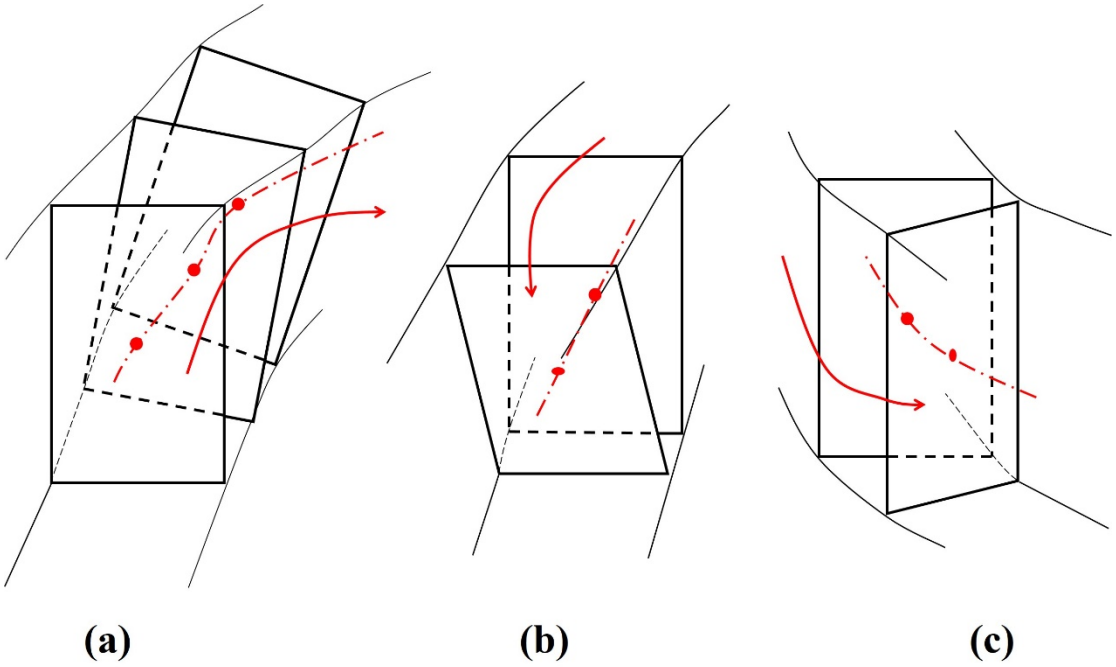

Fig. 3 Three types of twists in finite-sized coils, (a) surface twist, (b) edgewise bending and (c) flatwise bending. The red dash and dot line is the center line of the coil.

In Fig. 4, the red Cartesian coordinate (O-XYZ) is arbitrarily located and applied to describe spatial positions of each cross-section in a finite-sized coil. This coil comprises 48 poloidal cross-sections which are identical-shaped rectangles sketched in black color. The blue circle indicates an arbitrary cross-section of the coil. The other coordinate (r_G-uv) is fixed on the cross-section with the original point set in the center of this cross-section. Two axes OZ and $r_G v$ are employed to define the surface twist. β denotes the intersection angle between $\overrightarrow{OZ}$ and $\overrightarrow{r_G v}$. The definition of the surface twist is expressed by

$$\tau_s = cos\beta \tag{1}$$

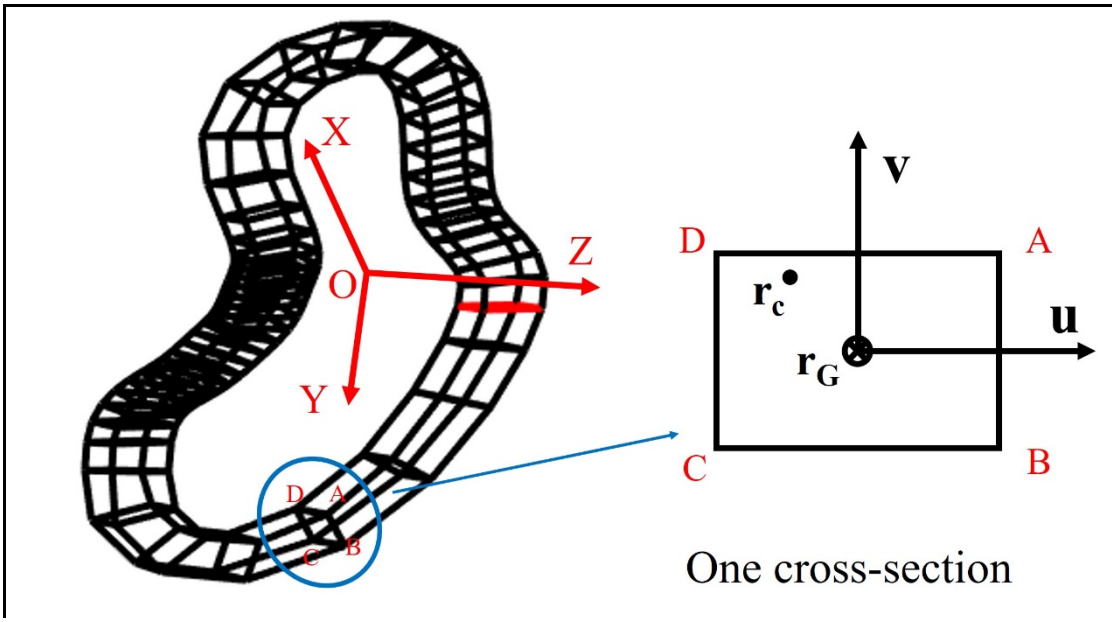

Fig. 4 Schematic diagram for a modular coil and a coil cross section marked by a blue cycle. Each modular coil has the same poloidal cross section, 132×69mm^2.

The position vector of an arbitrary point $\boldsymbol{r_c}$ on the modular coil cross-section is given by,

$$\boldsymbol{r_c}(l,\xi,\eta) = \boldsymbol{r_G} + \xi\boldsymbol{u} + \eta\boldsymbol{v} \tag{2}$$

Where $\boldsymbol{r_G}$ is the center point of the cross-section, $\boldsymbol{u}$ and $\boldsymbol{v}$ denote the unit vector along the $\overrightarrow{r_G u}$ and $\overrightarrow{r_G v}$ axes, respectively shown in Fig. 4. l represents the length of the coil at the center and used to determine positions of each coil cross-section. ξ and η are two components in the $\overrightarrow{r_G u}$ and $\overrightarrow{r_G v}$ directions.

Thus, the tangential vector at $\mathbf{r_c}$ can be written as,

$$\boldsymbol{t_c} \equiv \frac{d\boldsymbol{r_c}}{dl_c} = \left(\frac{d\boldsymbol{r_G}(l)}{dl} + \xi\frac{d\boldsymbol{u}(l)}{dl} + \eta\frac{d\boldsymbol{v}(l)}{dl}\right)\Big/\frac{dl_c}{dl} \tag{3}$$

$$-x_w \le \xi \le x_w \qquad -y_w \le \eta \le y_w$$

l_c is the length of the coil at the $\mathbf{r_c}$. x_w and y_w are the limitations of the half of length and width of the cross-section.

The curvature of the coil is given as follows,

$$\kappa = \left|\frac{d\boldsymbol{t_c}}{dl_c}\right| = \left|\frac{d^2\boldsymbol{r_c}}{dl_c^2}\right| \tag{4}$$

In order to definitely describe the line torsion of the coil, another pair of vectors are given,

$$\mathbf{b} = \mathbf{t_c} \times \mathbf{u}, \ \mathbf{n} = \mathbf{b} \times \mathbf{t_c} \tag{5}$$

Therefore, the line torsion is expressed by the following equation,

$$\tau_l = -\boldsymbol{n} \cdot \frac{d\boldsymbol{b}}{dl_c} \tag{6}$$

The basis ($\mathbf{t_c}$, **n**, **b**) are an orthonormal frame which is adequate to precisely describe the shape of a finite-sized coil with avoiding the Frenet–Serret frame [34,35] because this basis can be pathological in certain situations. The Frenet–Serret frame is revealed to be problematic if there are any points of vanishing curvature: even smooth curves can have discontinuous Frenet–Serret basis vectors [36]. The basis ($\mathbf{t_c}$, **n**, **b**) is temporarily called as the modified Frenet–Serret frame. In this paper, based on the modified Frenet-Serret frame, a new method has been applied to optimize the finite-sized coil shapes for the CFQS. The centerlines of the 16 coil packs are fixed during the entire optimization process. Five filaments in each coil are under consideration in the optimization process. These five filaments are set on the center and four edges of the coil cross-sections, respectively. The implement process is described as follows:

1. Initialize the reference coordinate and coil parameters, such as the position of the filament coil, the size of a practical coil cross-section, etc.
2. Arbitrarily twist each cross-section of coils and maintain all coil cross-sections torsion-free, i.e. set [Eq. (1)] = 0.0.
3. Calculate the line torsion [Eq. (6)], and curvature of the coil [Eq. (4)].
4. Rotate the reference coordinate by independently changing three Euler angles from 0-π, respectively.
5. Repeat process 2-4 and save cross-section data of all results.
6. Analyze data by a penalty function that reflects (a) the maximum curvature of the practical coil, (b) the average curvature of the practical coil, (c) the maximum surface twist of the practical coil, (d) the average surface twist of the practical coil, (e) the maximum line torsion of the practical coil, (f) the average line torsion of the practical coil. By using the error evaluation function, Eq. (7), error is estimated for each case.
7. From all results, choose the best one with a minimum error.

It is computed as

$$\rho = \sum_i w_i(x_i) \cdot \left(\frac{x_i - x_i^{design}}{x_i^{design}}\right)^2 \tag{7}$$

The x_i denote the actual quantities and x_i^{design} their ideal values. The $w_i(x_i)$ are weight functions for each of these quantities. In general, these weight functions are constants. Usually the magnitudes of the weight constants are chosen empirically[16].

4. Optimization results

The comparison of the initial reference coordinates and finally rotated ones are shown in Fig. 5. Figs. 5 (a), (b), (c) and (d) display reference coordinates which are utilized in the optimization of the MC1, MC2, MC3 and MC4 coils, respectively. The red coordinate is the original reference coordinate and the black is the optimized one. The Euler angle changes between the original and final reference coordinates are shown in Table. 1. The ψ, θ and φ represent precession, nutation and gyration angles, respectively. It is noted that the MC4 coil is the most complex coil. In order to considerably simplify it, the optimal reference coordinate is rotated (Fig. 5 (d)) with $\psi/2\pi=1.0786$, $\theta/2\pi=0.0838$ and $\varphi/2\pi=0.1553$. The largest rotation angle is the precession angle for the reference coordinate of the MC4 coil.

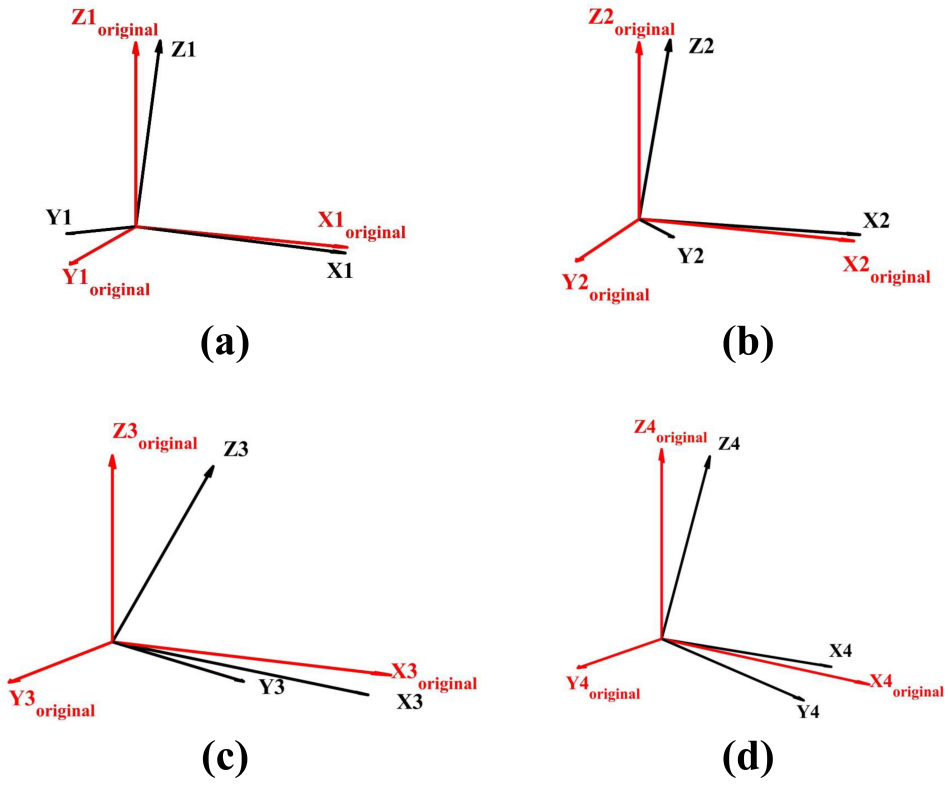

Fig. 5. The comparison of initial reference coordinates and final ones which are applied for optimization of MC1 (a), MC2 (b), MC3 (c) and MC4 (d) coils, respectively. The red ones are the original reference coordinates and the black are the optimized reference coordinates.

	Ψ/2π	θ/2π	φ/2π
M1	0.0244	0.1623	0.0663
M2	0.4276	0.1798	0.0838
M3	0.7906	0.096	0.2548
M4	1.0786	0.0838	0.1553

Table. 1 The Euler angles between the original and optimized coils' reference coordinates. The ψ, θ and φ are precession, nutation and gyration angles, respectively.

Via optimizations by this method, all surface twists of four finite-sized coils are completely suppressed. During the future fabrication of coils the winding frames and the coil cases will be manufactured more easily, which can be of great help to improve the coil manufacture accuracy. Figs. 6-9 show relevant parameters of the original and optimized coils. Without loss of generality five filaments in each coil are under consideration to calculate the related parameters. In Fig. 6, the original surface twists, line torsions and curvatures along the MC1 coil are given on the row (a) and corresponding parameters of the optimized MC1 coil are listed on the row (b). The horizontal axis represents the normalized poloidal angel of the coil. Regarding the original coil, the maximum line torsion and curvature are 10.960 rad/m and 22.890/m. After the optimization, the maximum values are decreased to 9.562 rad/m and 15.860/m, respectively. The similar results are also obtained in the surface twist optimizations of MC2, MC3, MC4 coils shown in Figs. 7-9, respectively. The line torsions and curvatures of a coil are primarily determined by the shape of the central filament of the coil. The central filament is kept fixed in the optimization process. Thus, the line torsions and curvatures of four edges are not improved significantly.

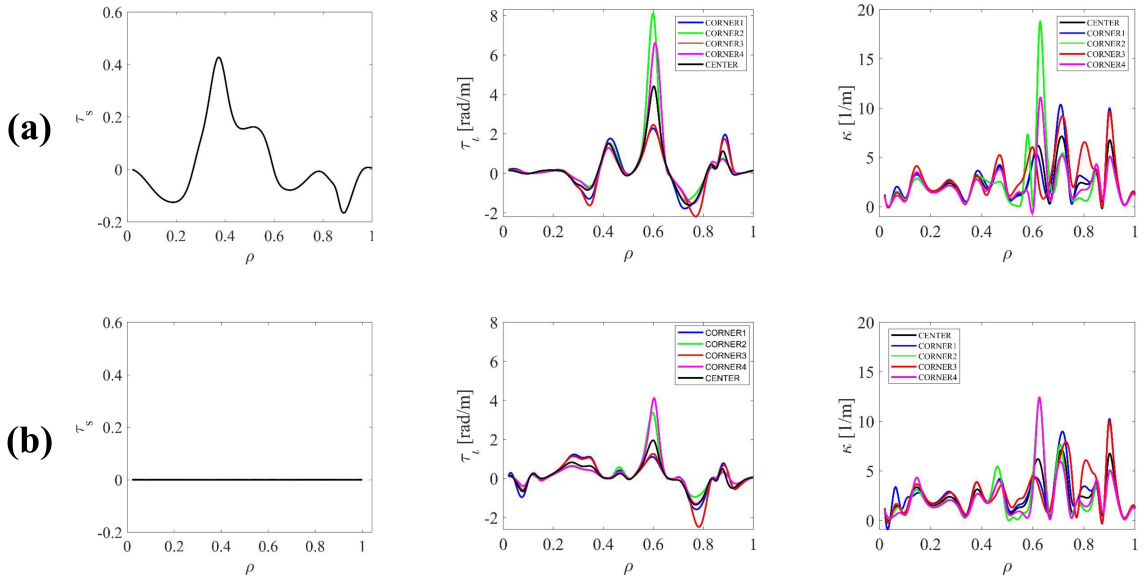

Fig. 6 The comparison of surface twists, line torsions and curvatures of the original (a) and optimized (b) MC1 coils, respectively

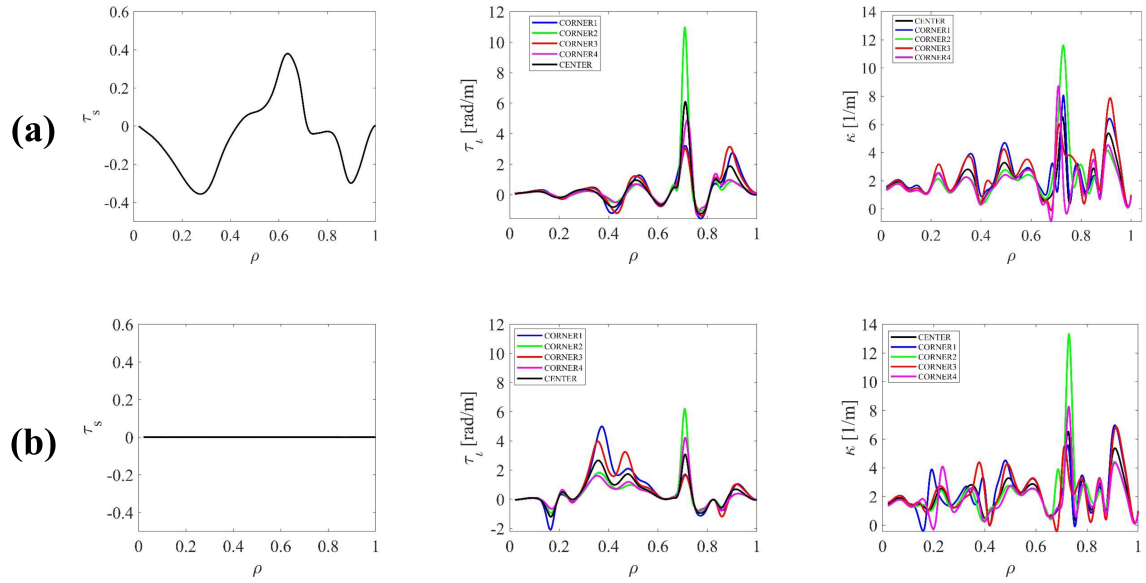

Fig. 7 The comparison of surface twists, line torsions and curvatures of the original (a) and optimized (b) MC2 coils, respectively

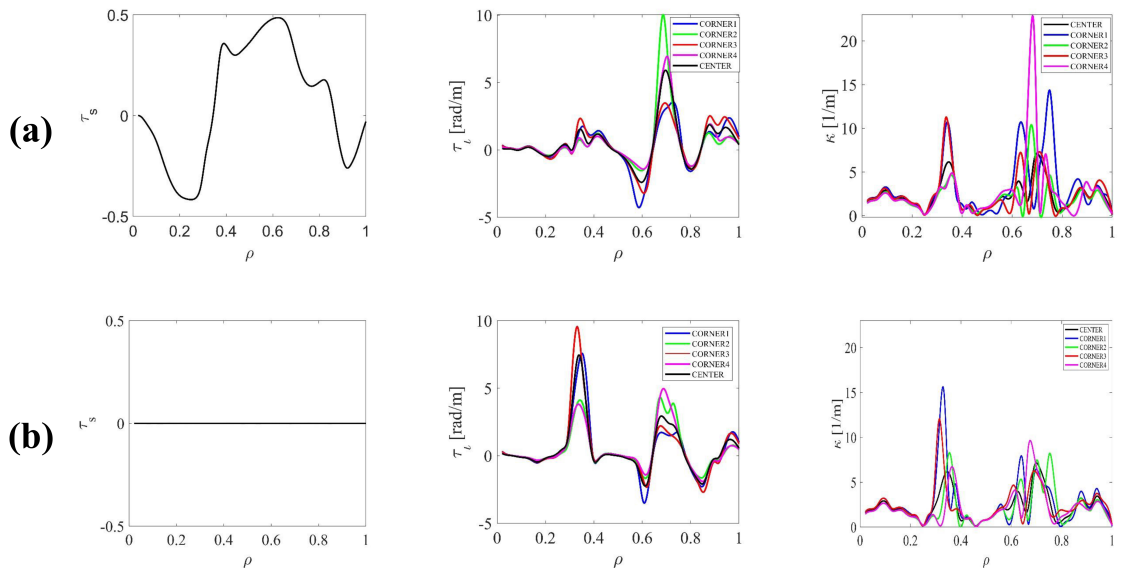

Fig. 8 The comparison of surface twists, line torsions and curvatures of the original (a) and optimized (b) MC3 coils, respectively

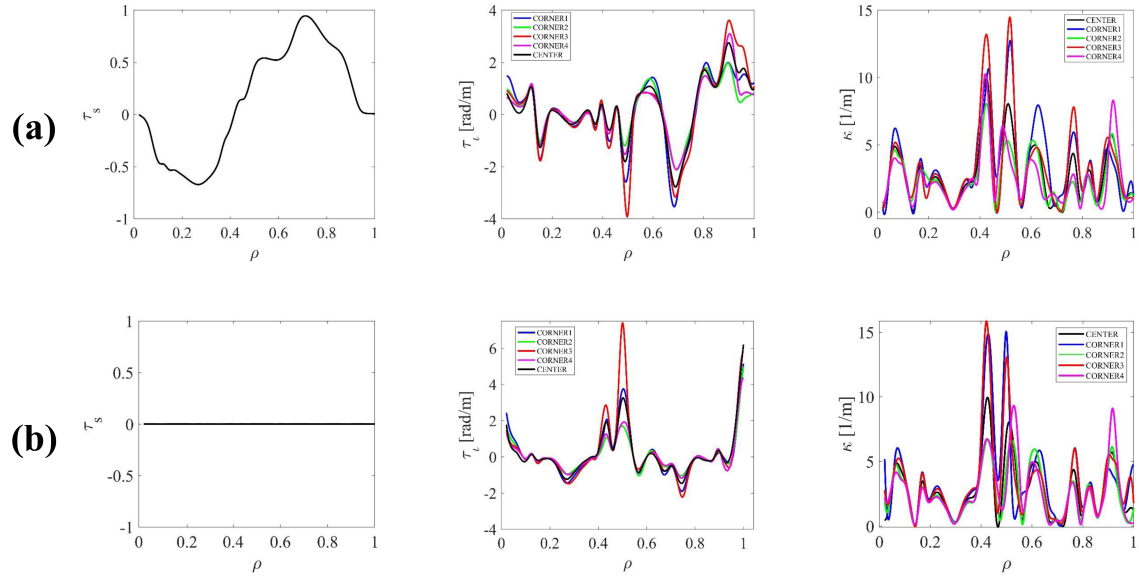

Fig. 9 The comparison of surface twists, line torsions and curvatures of the original (a) and optimized (b) MC4 coils, respectively

The forementioned figures illustrate that a set of surface-twist-free coils is perfectly achieved for the CFQS. Meanwhile, the line torsion and curvature are also decreased. In a certain direction view each finite-sized coil becomes planar-like one. Visually, the shapes of the optimized coils are shown in Fig. 10 (b). It clearly illustrates the surface twist of the original (a) and optimized (b) coils. Original coils all have obvious surface twist, while surface twists of the optimized coils are eliminated. In Fig.

10 (b) shown are optimized MC1, MC2, MC3 and MC4 coil of the CFQS in the $\overrightarrow{OZ}$ directions view which are black Z axes in Fig. 5. In this direction, each optimized finite-sized coil becomes planar-like one. Visually, the comparison of MC3 coil shapes between the original design (a) and surface-twist optimization (b) is given in Fig. 11. The blue dotted ellipses emphasize the regions with significant surface twists on the coil, which are in coincidence with results shown in Fig. 10. These regions are labeled with S1, S2 and S3, respectively. In Fig. 11(a) the toroidal twists among adjacent coil cross-sections are of significance at these regions, maximum τ_s = 0.5 as shown in Fig. 10. Via surface-twist optimizations these twists are effectively eliminated in Fig. 11(b). It exhibits a planar-like coil, which is very beneficial for fabrication of coil winding frames and coil cases.

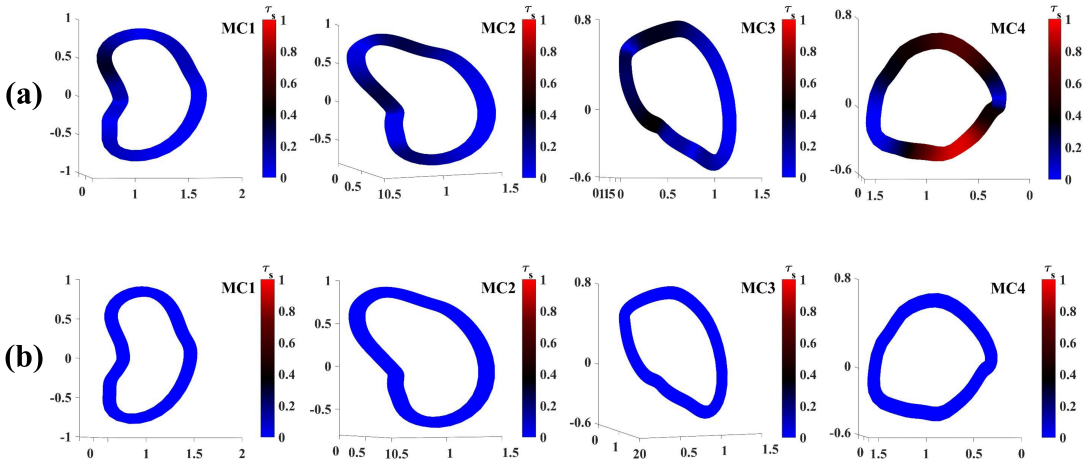

Fig.10 Shapes of the original (a) and optimized (b) coils. MC1, MC2, MC3 and MC4 coils of the CFQS are shown from the left to right side, respectively. The color bar represents surface twists of coils.

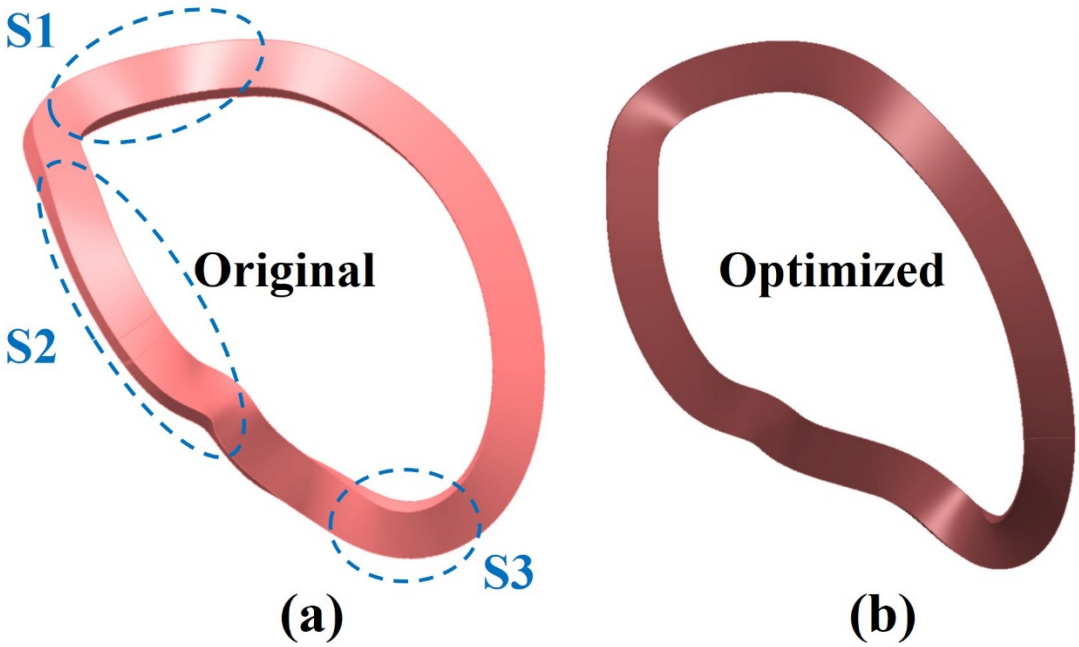

Fig. 11 The comparison of MC3 coil shapes between the original design (a) and surface-twist optimization (b). The blue dotted ellipses (S1, S2 and S3) emphasize the regions with significant surface twists on the original coil.

The purpose of the coil system is to precisely reproduce the designed magnetic field. In order to estimate the accuracy of the magnetic configuration induced by the practical coil system, the three kinds of coil-generated magnetic flux surfaces, and Fourier spectra of the magnetic field strength are computed. Figs. 12-13 displays these practical coils canonically generate the QA configuration by a multi-filament mode. The 3×3 filament currents are set in one coil to represent a finite-sized coil. The red curve represents the target plasma boundary calculated with the VMEC code. In Figs. 12 (a) – (c), Poincare plots of magnetic flux surfaces induced by the optimized finite-sized coils, unoptimized finite-sized coils, and filament coils, respectively, at the toroidal angles = 0°, 45° and 90°, which depict a good coincidence with the target plasma boundary. Each finite-sized coil has the same poloidal cross-section, 132.0×69.0 mm^2. It is indicated that in the CFQS the magnetic configuration is not sensitive to surface twist angles of coils and surface-twist-free coils could precisely reproduce the target magnetic field. Figs. 13 (a) - (c) depict the spectra of the magnetic field strength generated by the optimized finite-sized coil system, unoptimized finite-sized coil system and filament coil system, respectively. To distinguish small-amplitude

components, the largest component $B_{0,0}$ is omitted and the rest of components are normalized by the $B_{0,0}$ ($B_{m,n}$ / $B_{0,0}$). $B_{1,0}$ is the dominant component resulting from the toroidicity. Other components are much less than $B_{1,0}$, which shows a favorable quasi-axisymmetric configuration achieved by the optimized coils in Fig. 13(a). The amplitudes of main components of the target spectrum, the original coil-induced spectrum and the optimized coil-induced spectrum on the plasma boundary are listed in Table. 2. The definition of the deviation rate is (target $B_{m,n}$ – optimized coil-induced $B_{m,n}$) / target $B_{m,n}$. The deviation rate of subdominant component $B_{1,-1}$ is significant. Other components induced by optimized coils are very consistent with target ones. The deviation rates are all below 10%. Compared with the original coil design, this result is a more optimal coil system with much more accurate achievement of the magnetic configuration. Via the synthetical analyzation of Figs. 6 - 13 and Table 1, the surface-twist-free modular coils are perfectly achieved for the CFQS, more simplified than the original coil design and precisely reproduce the expected QA magnetic configuration.

Furthermore, interestingly, when a large-sized coil cross section is considered, even though central lines of all coil are fixed, the coil-induced configuration is sensitively influenced by the finite size of coils. Fig. 14 shows the one case Poincare plots of magnetic flux surfaces are generated by coils with a big-sized cross-section. The coil cross-section is enlarged to $103.5 \times 198 mm^2$. The red curve represents the target plasma boundary. There is no any magnetic flux surface induced by such coils overlapping with the expected boundary. The target configuration can’t be reproduced well by this set of modular coils. It shows that the deviation of magnetic fields are resulted from finite-size effects of coils.

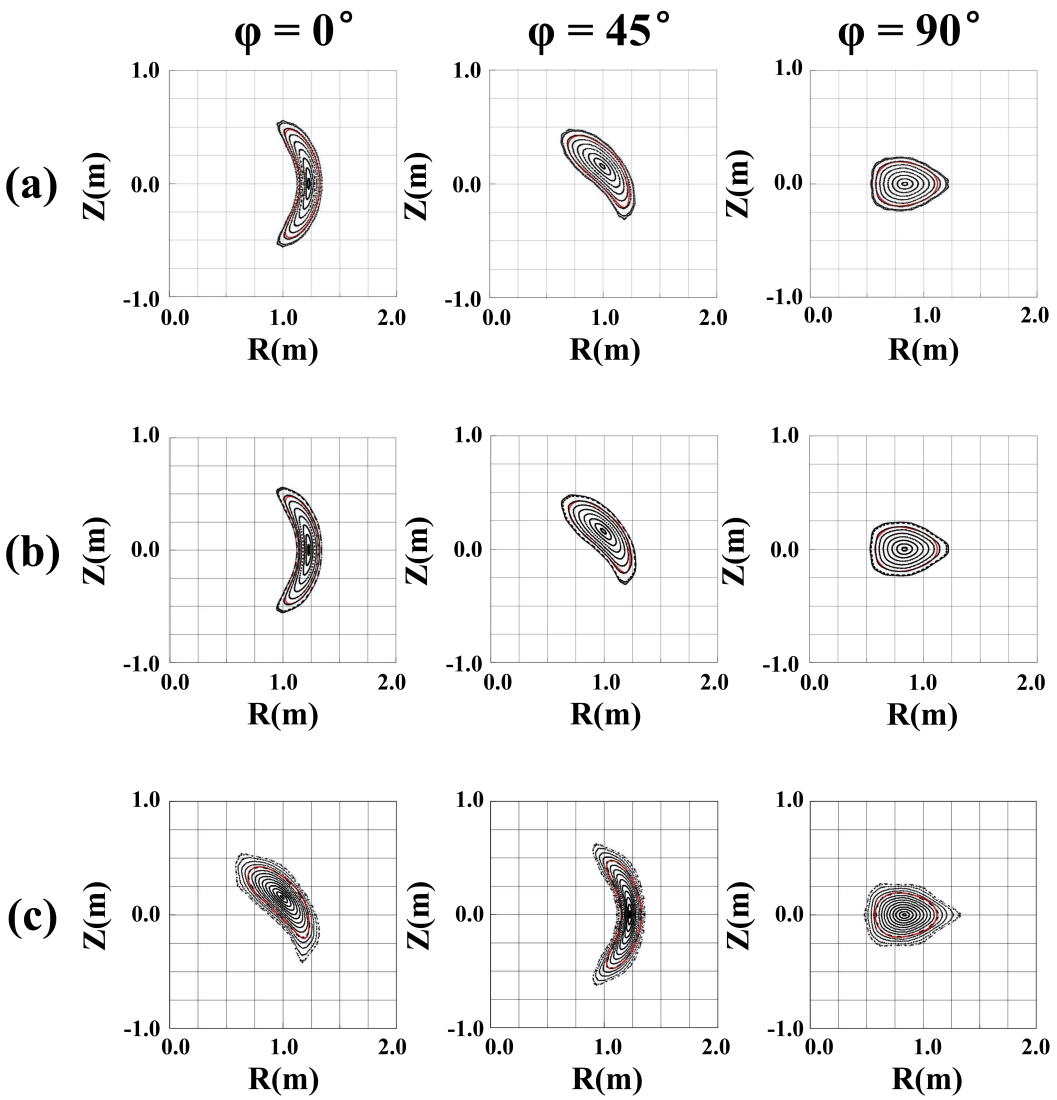

Fig. 12 Poincare plots of magnetic flux surfaces induced by the optimized finite-sized coils, unoptimized finite-sized coils, and filament coils ((a), (b) and (c), respectively) at the toroidal angle = 0°, 45° and 90°. The optimized and unoptimized coils are assumed to consist of 3×3 filament currents to induce magnetic configurations. The red curve represents the target plasma boundary calculated with the VMEC code.

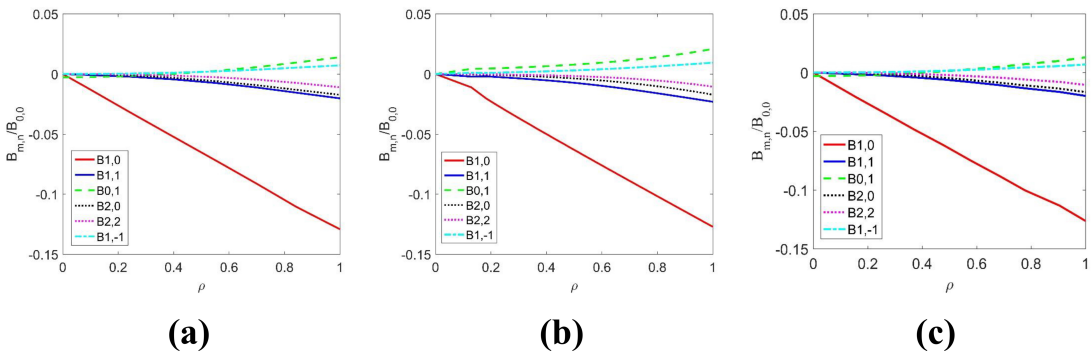

Fig. 13 The comparison of Fourier spectrum of the normalized magnetic field magnetic field strength in the Boozer coordinate frame for the CFQS (a) $B_{m,n}$ / $B_{0,0}$ generated with the optimized finite-sized coils. (b) $B_{m,n}$ / $B_{0,0}$ generated with the unoptimized finite-sized coils. (c) $B_{m,n}$ / $B_{0,0}$ generated with the filament coils.

Component	$B_{1,0}$ (T)	$B_{1,1}$ (T)	$B_{0,1}$ (T)	$B_{2,0}$ (T)	$B_{2,2}$ (T)	$B_{1,-1}$ (T)
Target	-0.1271	-0.0228	0.0205	-0.0169	-0.0106	0.0094
Original coil-induced	-0.1210	-0.0189	0.0125	-0.0158	-0.0100	0.0066
Optimized coil-induced	-0.1299	-0.0206	0.0143	-0.0180	-0.0115	0.0074
Deviation rate	2.2%	9.7%	3.02%	6.52%	9.28%	21.38%

Table. 2 Amplitudes of the target spectrum and spectrum induced by original coils and optimized coils.

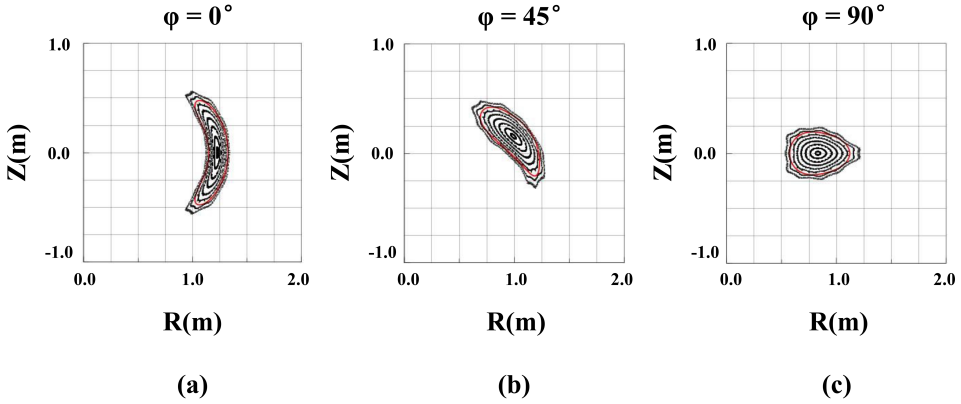

Fig. 14 Poincare plots of coil-generated magnetic flux surfaces at cross-section with φ = 0°, 45° and 90°. A big-sized coil cross-section is under consideration, 103.5×198 mm^2. One modular coil consists of 3×3 filaments. The red curves indicate the target plasma boundary calculated with the VMEC code.

5. Conclusion

In this paper, a new method is developed for the design of the practical coil system. Evolving from filament coils to finite-sized ones, each cross-section of coils is guaranteed perpendicular to the current carrying surface. That is to say that cross-

sections could twist toroidally along the central line of the coil. Thus, how to finalize the twisted angle for each cross-section plays a critical rule on the generation of practical coils, because these rotation angles significantly constrain the curvature radius, line torsion, surface twist of practical coils. The more important is that the magnetic configuration is very sensitive to these angles as well if the coil cross-section is big.

In this optimization, a rotatable Cartesian coordinate is utilized for the generation of arbitrary twisted angle variations for each cross-section of coils, which could include all probabilities of finite-sized coil shapes. Furthermore, in addition to the line torsion and curvature of coil, a new defined parameter, the surface twist, is included in the penalty function to calculate the toroidal twist scale of a cross-section relative to the adjacent cross-section. Specially setting the expression of the surface twist equal to 0, the optimized modular coils are completely surface-twist-free. This approach has been implemented to optimize the modular coil system of the CFQS. A practical coil system without any surface twists is accomplished shown in Fig. 10(b). Compared with the original coil design, this result is a more adequate coil system with the great simplification of coil shapes and precise achievement of the magnetic configuration.

Moreover, the finite-size effect of coils is of importance to achievement of ideal magnetic configurations and not avoidable. In future work, a couple of interesting topics are worthy to be investigated, e.g., (1) The effect of coil surface twist angles on the magnetic configuration; (2) The various cross section shapes of a coil influence the magnetic configuration and engineering constraints when the area of the cross section is fixed; (3) Coil surface twist angles can also be implemented for the estimation of stochastic deviations of practical coils during fabrication and assembly of the coil system; (4) How the finite-size of a coil effects the electro-magnetic force on coils and supporting structure.

Acknowledgments

The authors would like to acknowledge important discussions with Caoxiang Zhu. This work was partly supported by the National Key R&D Program of China under Grant Nos. 2017YFE0301705 and 2017YFE0300402 and National Natural Science Foundation of China under Grant No 11820101004.

Reference

[1] Spitzer 1981 *IEEE Trans. Plasma Sci.* **9**
[2] Xu Y. 2016 *Matter Radlat. Extrem.* **1** 192-200
[3] Lobsien J.-F.*, et al.* 2018 *Nucl. Fusion* **58**
[4] Sapper J. and Renner H. 1990 *Fusion Sci. Technol* **17** 62-75
[5] Ku L. P. and Boozer A. H. 2010 *Nucl. Fusion* **50**
[6] Rummel T.*, et al.* 2005 *Fusion Eng. Des.* **75** 117-121
[7] Dinklage A.*, et al.* 2018 *Nat. Phys.* **14** 855-860
[8] Anderson F. S. B.*, et al.* 2018 *Fusion Sci. Technol.* **27** 273-277
[9] Almagri A. F.*, et al.* 1999 *IEEE Trans. Plasma Sci.* **27** 114-115
[10] Isobe M.*, et al.* 2019 *Plasma Fusion Res.* **14** 3402074-3402074
[11] Liu H.*, et al.* 2018 *Plasma Fusion Res.* **13** 3405067-3405067
[12] Xu Y.*, et al. Proc. of 27th IAEA Fus. Energy Conf., Ahmedabad, India,* 2018.
[13] Merkel P. 1987 *Nucl. Fusion* **27** 867
[14] Pomphrey 2001 *Nucl. Fusion* **41**
[15] Matt 2017 *Nucl. Fusion* **57**
[16] Drevlak M. 2018 *Fusion Sci. Technol* **33** 106-117
[17] Drevlak M. 1999 *Proc. of the 12th Int. Stellarator Workshop* (*27 Septermber–1 October 1999*) pp 1–17
(www-fusion.ciemat.es/SW2005/conferences/madison99/Papers/drevlak.pdf)
[18] Strickler D. J.*, et al.* 2002 *Fusion Sci. Technol.* **41** 107-115
[19] Brown T., *et al.* 2015 *IEEE 26th Symp. on Fusion Engineering* pp 1–6
[20] Zarnstorff M.C. *et al.* 2001 *Plasma Phys. Control. Fusion* 43 237–49
[21] Nelson B. E. *et al.* 2003 *Fusion Eng. Des.* **66** 169-174
[22] Shimizu A., *et al.* 2003 *Fusion Eng. Des.* **65** 109-118
[23] Nemov V.V. *et al.* 2003 *Plasma Phys. Control. Fusion* **45** 1829–1843
[24] Zhu C.*, et al.* 2018 *Nucl. Fusion* **58**
[25] Zhu C.*, et al.* 2019 *Nucl. Fusion* **59**
[26] Shimizu A.*, et al.* 2018 *Plasma Fusion Res.* **13** 3403123-3403123
[27] Boozer A. H. 2009 *phys. plasma* **16** 058102
[28] Nührenberg J. 2010 *Plasma Phys. Control. Fusion* **52** 124003
[29] Spong D. A. 2015 *phys. plasma* **22** 055602
[30] Sanchez R., *et al.* 2000 *Plasma Phys. Control. Fusion* **42** 641
[31] Hirshman 1983 *Phys. Fluids* **26**
[32] Kinoshita S.*, et al.* 2019 *Plasma Fusion Res.* **14** 3405097-3405097
[33] Abadoğlu E. and Gūmral H. 2009 *Physica D* **238** 526-530
[34] Garren D. A. and Boozer A. H. 1991 *Physics of Fluids B: Plasma Physics* **3** 2805-2821
[35] Garren D. A. and Boozer A. H. 1991 *Physics of Fluids B: Plasma Physics* **3** 2822-2834
[36] Landreman M. and Sengupta W. 2018 J. Plasma Phys, 84, 905840616